



## Deposition Velocity onto an Inverted Flat Surface in a Laminar Parallel Flow

Woo-Joo Choi & Se-Jin Yook

To cite this article: Woo-Joo Choi & Se-Jin Yook (2010) Deposition Velocity onto an Inverted Flat Surface in a Laminar Parallel Flow, *Aerosol Science and Technology*, 44:11, 919-929, DOI: [10.1080/02786826.2010.501833](https://doi.org/10.1080/02786826.2010.501833)

To link to this article: <https://doi.org/10.1080/02786826.2010.501833>



Published online: 23 Aug 2010.



Submit your article to this journal [↗](#)



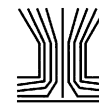
Article views: 763



View related articles [↗](#)



Citing articles: 1 View citing articles [↗](#)



# Deposition Velocity onto an Inverted Flat Surface in a Laminar Parallel Flow

Woo-Joo Choi and Se-Jin Yook

*School of Mechanical Engineering, Hanyang University, Seongdong-gu, Seoul, Republic of Korea*

Wafers and photomasks in the cleanroom are exposed to airflows not only vertical but also parallel to the surfaces. In this study, Gaussian Diffusion Sphere Model (GDSM) was adjusted to predict deposition velocity onto an inverted flat surface in a laminar parallel flow by considering Brownian diffusion and gravitational settling of aerosol particles. The GDSM was validated by comparing with the simulation of solving flow and aerosol-concentration fields for an inverted flat surface and also with the mass transfer correlation for a finite flat surface of circular or rectangular areal shape. The GDSM was proven to correctly predict the deposition velocities onto the inverted flat surfaces, by taking one hour with a 2.66-GHz-CPU personal computer to obtain deposition velocities for 20 particle sizes, which is a very much shorter time compared with the time for simulating the flow and aerosol-concentration fields. Deposition velocities onto the inverted 45-cm-wafer and 15.2-cm-photomask in parallel airflows were predicted using the GDSM, for the particle size ranging from 0.003 to 1.5  $\mu\text{m}$  and the airflow velocity varying from 5 to 500 cm/s. The deposition velocity decreased with increasing particle size, with a steep declination especially for particles larger than approximately 0.1  $\mu\text{m}$ . From the qualitative comparison of the deposition velocities onto the inverted square flat surfaces, representing the photomasks with different orientations in the parallel flow, it was suggested to transport the EUVL photomask with its side facing the airflow rather than with its corner confronting the airflow, in order to minimize particulate contamination.

## 1. INTRODUCTION

Extreme Ultraviolet Lithography (EUVL) is thought of as the likely technology for making half-pitch nodes smaller than 32 nm (Kemp and Wurm 2006). Since the pellicles cannot be used in the EUVL technology, photomasks are vulnerable to particulate contamination (Yook et al. 2007a). The control of particulate contamination is therefore getting critical in enhancing the product yield in semiconductor manufacturing, as the

feature size shrinks. Deposition velocity, defined as the ratio of particle flux toward a surface to aerosol concentration above that surface, is accepted as the criterion to assess the level of particulate contamination. Previous researches of deposition velocity have focused on the horizontal free-standing wafer to which air flow is perpendicular (Liu and Ahn 1987; Opiolka et al. 1994; Otani et al. 1989; Pui et al. 1990; Ye et al. 1991; Yook et al. 2007b). Since horizontal wafers or photomasks are transported horizontally by robots in the cleanroom, aerosol particles may approach and contaminate the wafers or photomasks by the air flow parallel to the surfaces. After Liu and Ahn (1987), however, not many studies have paid attention to deposition velocity onto the wafers or photomasks in parallel flows.

Fast and correct prediction of deposition velocity is important to quickly and rightly evaluate the level of particulate contamination. Many researchers developed simple models for predicting deposition velocity onto smooth or rough surfaces, based on the friction velocity of a turbulent flow (Wood 1981; Lai and Nazaroff 2000; Zhao and Wu 2006a, 2006b). By considering the sizes of wafers or photomasks and the speeds of horizontal transportation in semiconductor manufacturing, however, the flow developing over the wafer or photomask surface is laminar. Recently, Yook and Ahn (2009) developed the Gaussian Diffusion Sphere Model (GDSM), which predicts mean mass transfer coefficient onto a flat surface exposed to a laminar parallel flow by considering Brownian diffusion of aerosol particles and estimating deposition probabilities of particles diffusing in the boundary layer. The GDSM was employed to obtain correlations of mean Sherwood numbers for finite flat plates of various areal shapes such as square, rectangle, circle, ellipse, and rhombus, by varying plate shape, plate size, aspect ratio, free-stream velocity and kind of fluid in wide ranges of Schmidt number and fluid temperature (Yook et al. 2010a). The GDSM was adjusted to predict deposition velocity onto a face-up, flat surface in a parallel flow when both Brownian diffusion and gravity enhanced particle deposition (Yook et al. 2010b). The GDSM was proven to be correct even though it took very much shorter time compared with the time required for the simulation of solving flow and aerosol-concentration fields.

One of the schemes to minimize particulate contamination of EUVL photomasks is the use of the gravity by letting the

Received 22 February 2010; accepted 7 June 2010.

This work was supported by the research fund of Hanyang University (HY-2009-O). The authors would like to thank Mr. Ki-Hwan Kim and Mr. Sang-Bum Lee for fruitful discussion.

Address correspondence to Se-Jin Yook, School of Mechanical Engineering, Hanyang University, 17 Haengdang-dong, Seongdong-gu, Seoul 133-791, Republic of Korea. E-mail: ysjnuri@hanyang.ac.kr

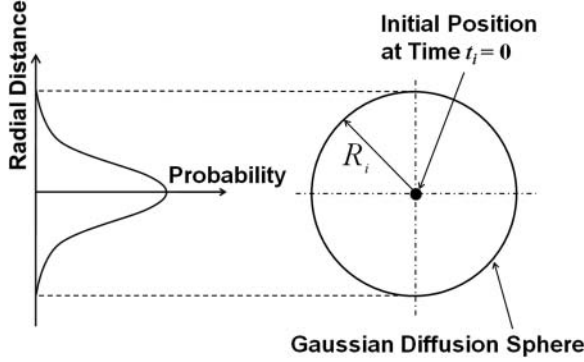


FIG. 1. Concept of the Gaussian Diffusion Sphere.

critical surfaces facing down (Asbach et al. 2006; Yook et al. 2007b, 2007c). It is thus helpful to render the critical surfaces of wafers or photomasks facing-down even at the stages of transporting them by robots. It usually requires much effort and time to estimate deposition velocities by solving flow and aerosol-concentration fields for many combinations of wafer/photomask size and transportation speed. Therefore, the objective of this study is to develop a simple model which can be used to quickly and correctly assess the level of particulate contamination, by adjusting the GDSM to predict deposition velocity onto an inverted flat surface, e.g., face-down wafers or photomasks, in a laminar parallel flow, when the gravity suppresses particle deposition.

## 2. GAUSSIAN DIFFUSION SPHERE MODEL FOR INVERTED FLAT SURFACES

### 2.1. Concept of Gaussian Diffusion Sphere

Airborne particles diffuse randomly and the behavior of a diffusing particle can be treated with a statistical approach. As shown in Figure 1, the Gaussian Diffusion Sphere (GDS) portrays the space within which a particle can diffuse after a certain time ( $t_i$ ). The center of GDS represents the initial particle position at  $t_i = 0$ . The displacement of the particle at each moment is weighted by a Gaussian probability density function of which standard deviation ( $\sigma_i$ ) is equal to the root-mean-square net displacement by diffusion (Hinds 1999), i.e.,

$$\sigma_i = \sqrt{2Dt_i}, \quad [1]$$

where the subscript “ $i$ ” denotes the  $i$ -th element in  $x$ -direction (Figure 6), and  $D$  is the particle diffusivity. The radius of GDS is expressed as

$$R_i = n_\sigma \sigma_i, \quad [2]$$

where  $n_\sigma$  is an integer for determining the confidence interval. In other words,  $R_i$  represents the radius of a sphere within which a particle, diffusing from its initial position at  $t_i = 0$ , can

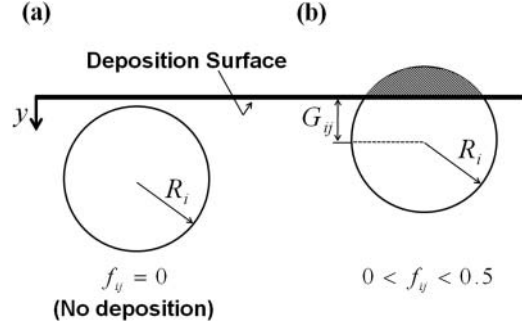


FIG. 2. Two representative cases of the overlap of GDS with an inverted deposition surface.

be located after a certain time by considering the confidence interval, e.g.,  $n_\sigma$  of 2 represents 95% confidence interval.

Figure 2 shows two representative cases of the overlap of the GDS with an inverted surface, as suggested by Asbach et al. (2008). If the GDS does not meet the surface, it points out that the particle is unable to reach the surface by diffusion within a certain time and therefore the deposition probability ( $f_{ij}$ ) is zero. If the GDS overlaps with the surface, it implies that the particle may deposit on the surface by diffusion within a certain time. The deposition probability can be estimated as (Yook and Ahn 2009)

$$f_{ij} = \frac{1}{2} \left\{ \operatorname{erf} \left( \frac{R_i}{\sqrt{2}\sigma_i} \right) - \operatorname{erf} \left( \frac{G_{ij}}{\sqrt{2}\sigma_i} \right) \right\} - \left( \frac{R_i - G_{ij}}{\sqrt{2\pi}\sigma_i} \right) \exp \left( -\frac{R_i^2}{2\sigma_i^2} \right), \quad [3]$$

where  $G_{ij}$  is the distance between the GDS center and deposition surface. If the GDS center is placed on the surface, i.e.,  $y = 0$ , the probability-weighted volume of GDS overlapping with the surface becomes hemispherical, and thus  $f_{ij} = 0.5$ . Since the initial particle location is under the surface and the gravity acts downward, the GDS center cannot cross the deposition surface and therefore the deposition probability ranges from 0 to 0.5.

### 2.2. Determination of Concentration Boundary Layer Thickness

A flow boundary layer develops when the air flows under an inverted deposition surface, as shown in Figure 3a. The free-stream air velocity is  $U$ . The length of the deposition surface is  $L_i$ . The approximated flow velocity profile is given as (Holman, 2010)

$$u = U \left[ \frac{3}{2} \left( \frac{y}{\delta_{f,z}} \right) - \frac{1}{2} \left( \frac{y}{\delta_{f,z}} \right)^3 \right] \quad (\text{if } y \leq \delta_{f,z}), \quad [4a]$$

$$u = U \quad (\text{if } y > \delta_{f,z}), \quad [4b]$$

where  $u$  is the flow velocity in  $z$ -direction and  $\delta_{f,z}$  is the flow boundary layer thickness. For the simplicity, the flow velocity

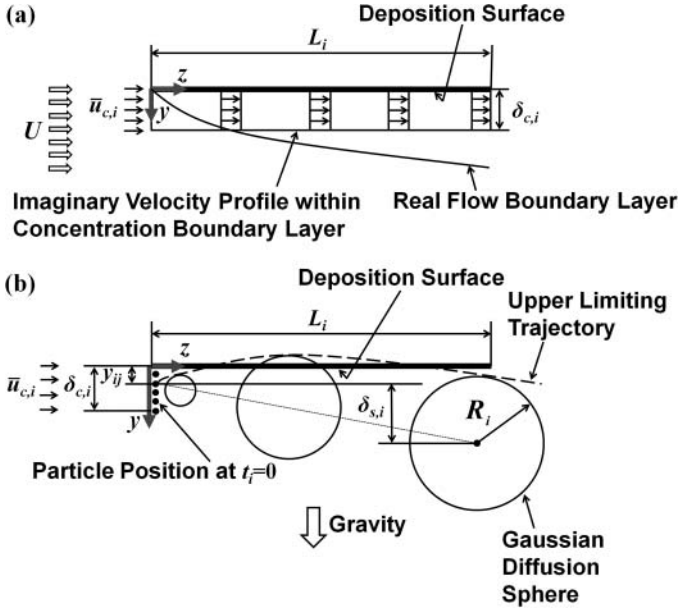


FIG. 3. Schematic for calculating deposition velocity onto an inverted flat surface: (a) imaginary flow velocity profile within concentration boundary layer; (b) evolution of GDS with time when Brownian diffusion and gravitational settling are simultaneously considered.

in  $y$ -direction is assumed to be

$$w = 0. \quad [4c]$$

The flow boundary layer thickness is calculated as

$$\delta_{f,z} = \frac{5z}{Re_z^{1/2}} = 5\sqrt{\frac{\nu z}{U}}. \quad [5]$$

where  $Re(=Uz/\nu)$  is the Reynolds number and  $\nu$  is the kinematic viscosity of air. In general, for an aerosol flow, the thickness of the concentration boundary layer is much thinner than that of the flow boundary layer (Otani et al. 1989). Therefore, the flow velocity profile near the deposition surface, i.e., within the concentration boundary layer, is assumed to be linear. The mean flow velocity within the concentration boundary layer is calculated as

$$\bar{u}_{c,i} = \frac{1}{L_i \delta_{c,i}} \int_{z=0}^{L_i} \int_{y=0}^{\delta_{c,i}} u \, dy \, dz = \frac{3\delta_{c,i}}{10} \sqrt{\frac{U^3}{\nu L_i}}. \quad [6]$$

In this study, it is assumed that only the particles injected within  $\delta_{c,i}$  at the leading edge may deposit on the surface. In other words, the deposition probability of the particle initially located outside  $\delta_{c,i}$  is zero. Note that  $\delta_{c,i}$  is constant along the flow direction as illustrated in Figure 3a. The flow residence time within  $\delta_{c,i}$  beneath the plate of length  $L_i$  in a parallel flow

of velocity  $U$  is

$$t_i = \frac{L_i}{\bar{u}_{c,i}} = \frac{a_i}{\delta_{c,i}}, \quad [7]$$

where

$$a_i = \frac{10}{3} \sqrt{\frac{\nu L_i^3}{U^3}}. \quad [8]$$

Figure 3b illustrates the evolution of GDS, as a particle drifts toward the trailing edge by the airflow of mean velocity  $\bar{u}_{c,i}$  within  $\delta_{c,i}$ . The GDS becomes larger with time due to diffusion. Since the deposition surface is facing down, the gravity let the particle move away from the surface and therefore the center of the GDS drops down. It is assumed that the particle velocity in  $z$ -direction is the same as the flow velocity and that it momentarily attains its terminal settling velocity in  $y$ -direction. The settling distance ( $\delta_{s,i}$ ) of the GDS with time can be calculated as (Hinds 1999)

$$\delta_{s,i} = v_s t_i, \quad [9]$$

where  $v_s$  is the settling velocity, or

$$v_s = \frac{\rho_p d_p^2 C_c g}{18\mu}. \quad [10]$$

Here,  $\rho_p$  is the particle density,  $d_p$  is the particle size,  $C_c$  is the slip correction factor,  $g$  is the gravitational acceleration, and  $\mu$  is the viscosity of air. If the particle is initially located at a distance of  $y_{ij}$  away from the surface at the leading edge, the instant distance between the GDS center and the deposition surface, i.e.,  $G_{ij}$ , is calculated as

$$G_{ij} = y_{ij} + \delta_{s,i}. \quad [11]$$

Note that  $G_{ij}$  changes with time due to gravitational settling.

The maximum fraction of GDS overlapping with the deposition surface, i.e.,  $\max(f_{ij})$ , determines the probability of the particle initially started at the distance of  $y_{ij}$  from the surface at the leading edge. Since the gravity works against particle deposition as considered in this study, the maximum fraction of overlap may show up while the GDS passes under the deposition surface as illustrated in Figure 3b, depending on the particle size. Therefore, it is necessary to find out where the maximum fraction of overlap makes an appearance.

Since the GDS represents the circumscription within which the particle in question can be displaced after a certain time  $t_i$ , the concentration boundary layer thickness, or  $\delta_{c,i}$ , can be determined by observing the upper limiting trajectory of GDS, which is depicted using a dashed curve in Figure 3b. The upper limiting trajectory of GDS for the particle initially injected at

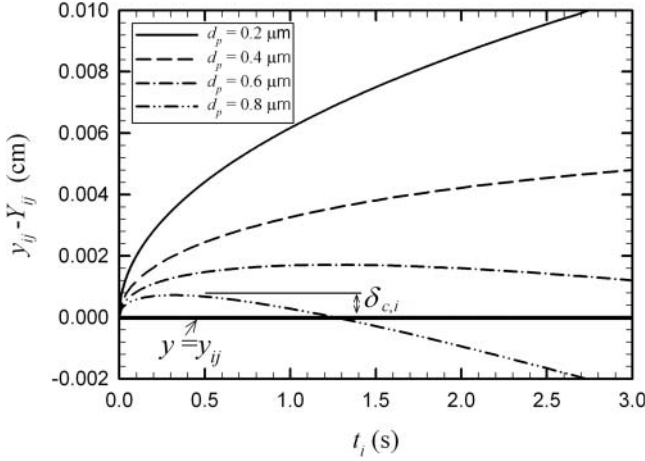


FIG. 4. Upper limiting trajectories of GDS.

$y = y_{ij}$  can be expressed as

$$Y_{ij} = y_{ij} - R_i + \delta_{s,i}. \quad [12]$$

If the upper limiting trajectory of GDS does not touch the deposition surface, it means that the particle in question can never reach the surface. Thus, the concentration boundary layer thickness is determined by finding out the critical upper limiting trajectory that exactly comes in contact with the deposition surface. In other words, the maximum value of  $(y_{ij} - Y_{ij})$ , corresponding to the given values of  $d_p$ ,  $L_i$ , and  $U$ , becomes the concentration boundary layer thickness, or

$$\delta_{c,i} = \max(y_{ij} - Y_{ij}) = \max(n_\sigma \sqrt{2Dt_i} - v_s t_i). \quad [13]$$

As an example, Figure 4 shows the upper limiting trajectories of GDS for several particle sizes as a function of time, in reference to the initial particle location at  $y_{ij}$ . When  $d_p = 0.2 \mu\text{m}$ , the effect of Brownian diffusion is relatively large compared to that of gravitational settling. As a result, the upper limiting trajectory of GDS for the  $0.2\text{-}\mu\text{m}$ -particle assumes an upward curve, which means the concentration boundary layer thickness is determined from the value of  $t_i$  at the end of the surface. When  $d_p = 0.8 \mu\text{m}$ , the effect of gravitational settling is relatively large, and the upper limiting trajectory of GDS reaches the summit and goes down. In this example, the concentration boundary layer thickness for the  $0.8\text{-}\mu\text{m}$ -particle is determined using the value of  $t_i$  at the inflection of  $Y_{ij}$  as illustrated in Figure 4. Note that the concentration boundary layer thickness depends on not only the particle size but also the residence time of the particle within  $\delta_{c,i}$  beneath the deposition surface. Namely, if the plate length is short enough for the residence time of the  $0.8\text{-}\mu\text{m}$ -particle within the concentration boundary layer to be, say,  $0.1 \text{ s}$ , then  $\delta_{c,i}$  can be obtained using the value of  $t_i$  at the end of the surface. This implies that it is critical to figure out whether the inflection of  $Y_{ij}$  occurs during the particle drift under the deposition surface or not.

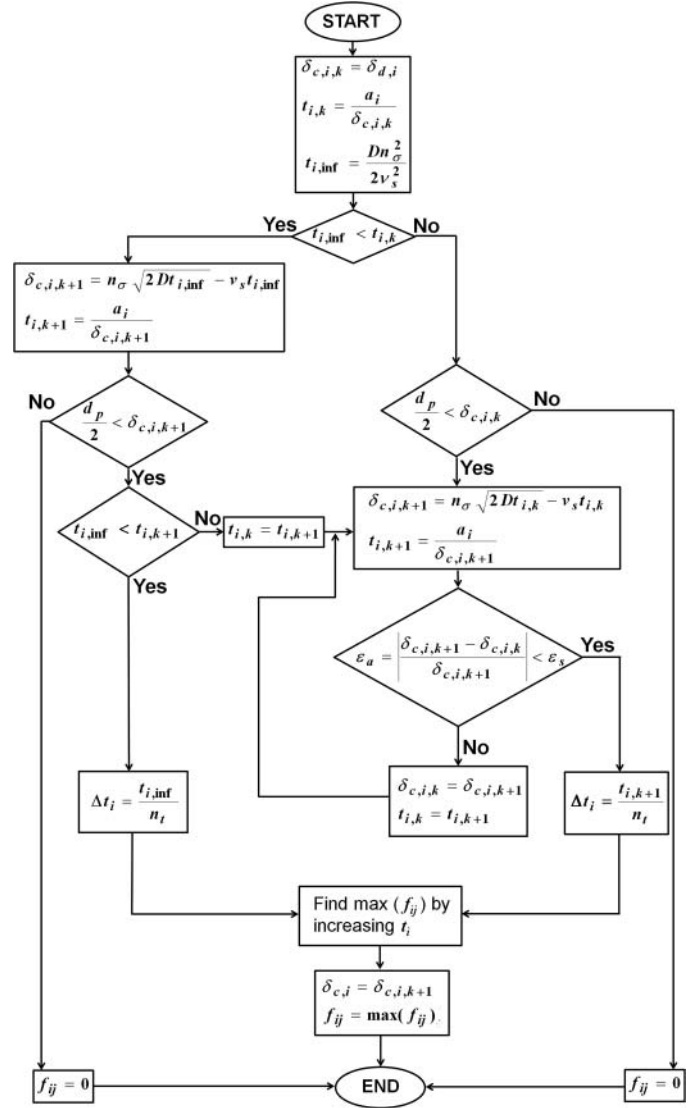


FIG. 5. Flowchart for determining the concentration boundary layer thickness and the particle deposition probability using the GDSM for an inverted flat surface.

Figure 5 shows a flowchart for determining the concentration boundary layer thickness and deposition probability beneath an inverted flat surface, for a particle size. The particle drifts in  $z$ -direction by the flow and at the same time in  $y$ -direction due to gravity, which requires an iterative method for determining the concentration boundary layer thickness by reflecting the effects of both Brownian diffusion and gravitational settling. Initial guess of  $\delta_{c,i}$  is made by considering only Brownian diffusion, i.e., by assuming that the concentration boundary layer thickness is equal to the diffusion boundary layer thickness ( $\delta_{d,i}$ ), which is obtained as (Cengel, 2003)

$$\delta_{c,i,k} = \delta_{d,i} = \frac{5L_i}{Re_{L_i}^{1/2} Sc^{1/3}}. \quad [14]$$

Here, the subscript “ $k$ ” denotes the previous value in the iterative calculation,  $Re_{Li}(= UL_i/\nu)$  is the Reynolds number, and  $Sc(= \nu/D)$  is the Schmidt number. From Equation (7), the flow residence time within  $\delta_{c,i,k}$  is

$$t_{i,k} = \frac{a_i}{\delta_{c,i,k}}. \quad [15]$$

The time for the upper limiting trajectory of GDS to reach the point of inflection is obtained by differentiating Equation (12) with respect to  $t_i$  and then setting  $dY_{ij}/dt_i = 0$ , or

$$t_{i,\text{inf}} = \frac{Dn_\sigma^2}{2v_s^2}, \quad [16]$$

where the subscript “inf” denotes the point of inflection. In order to make an estimation whether the point of inflection appears during the particle drift under the deposition surface or not,  $t_{i,\text{inf}}$  is compared with  $t_{i,k}(= a_i/\delta_{d,i})$ .

If  $t_{i,\text{inf}}$  is smaller than  $a_i/\delta_{d,i}$ , then it implies that the upper limiting trajectory of GDS may reach its summit while it travels underneath the deposition surface. Based on the discussion about Figure 4, the concentration boundary layer thickness can be calculated by substituting  $t_{i,\text{inf}}$  to Equation (13), or

$$\delta_{c,i,k+1} = n_\sigma \sqrt{2Dt_{i,\text{inf}}} - v_s t_{i,\text{inf}}, \quad [17]$$

where, the subscript “ $k+1$ ” denotes the current value in the iterative calculation. The particle residence time within the newly obtained concentration boundary layer thickness is

$$t_{i,k+1} = \frac{a_i}{\delta_{c,i,k+1}}. \quad [18]$$

By considering the physical size of the particle, the concentration boundary layer needs to be thicker than the particle radius. In order to judge whether the point of inflection of  $Y_{ij}$  still shows up during the particle drift beneath the inverted surface under the consideration of both Brownian diffusion and gravitation settling,  $t_{i,\text{inf}}$  is compared with  $t_{i,k+1}\{= a_i/[n_\sigma(2Dt_{i,\text{inf}})^{1/2} - v_s t_{i,\text{inf}}]\}$ .

If  $t_{i,\text{inf}}$  is smaller than  $a_i/[n_\sigma(2Dt_{i,\text{inf}})^{1/2} - v_s t_{i,\text{inf}}]$ , then the inflection point of  $Y_{ij}$  makes an appearance while the particle passes under the inverted surface and the concentration boundary layer thickness is determined as  $\delta_{c,i} = n_\sigma(2Dt_{i,\text{inf}})^{1/2} - v_s t_{i,\text{inf}}$ . The maximum fraction of GDS overlapping with the deposition surface, i.e., the deposition probability of the particle initially positioned at  $y_{ij}$  at the leading edge, is found by increasing the time  $t_i$  from 0 to  $t_{i,\text{inf}}$  with the time step of  $\Delta t_i = t_{i,\text{inf}}/n_t$ , where  $n_t$  is the number of grids for determining the time increment.

If  $t_{i,\text{inf}}$  is larger than  $a_i/\delta_{d,i}$  or  $a_i/[n_\sigma(2Dt_{i,\text{inf}})^{1/2} - v_s t_{i,\text{inf}}]$ , then it implies that the inflection point of  $Y_{ij}$  is absent while the particle travels beneath the plate of length  $L_i$ . In this case,  $\delta_{c,i}$  is calculated from the value of  $t_i$  at the end of the surface. The

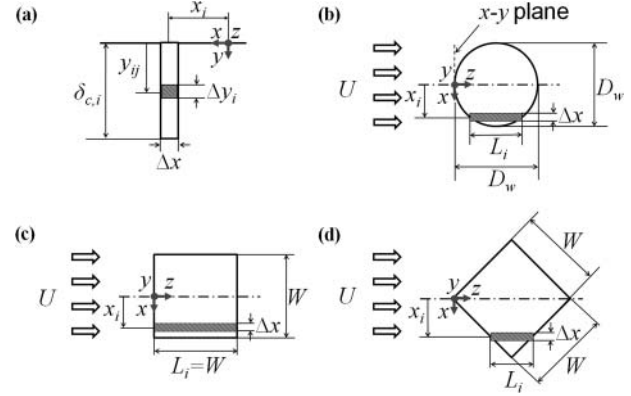


FIG. 6. Schematic of the GDSM procedure for calculating deposition velocity onto an inverted finite flat surface: (a) view from the  $x$ - $y$  plane; (b) top view of a circular flat surface; (c) top view of a square flat surface with its side facing the flow; (d) top view of a square flat surface with its corner facing the flow.

concentration boundary layer thickness  $\delta_{c,i}$  can be obtained by iteratively finding out the particle residence time  $t_{i,k+1}$  under the effects of both Brownian diffusion and gravitational settling, until the percent relative error  $\varepsilon_a$  becomes smaller than the prespecified acceptable level  $\varepsilon_s$ . Once the value of  $\delta_{c,i,k+1}$  converges, the concentration boundary layer thickness is determined as  $\delta_{c,i} = \delta_{c,i,k+1}$ . Then, the deposition probability, i.e.,  $\max(f_{ij})$ , is found by increasing the time  $t_i$  from 0 to  $t_{i,k+1}(= a_i/\delta_{c,i,k+1})$  with the time step of  $\Delta t_i = t_{i,k+1}/n_t$ .

### 2.3. Calculation of Deposition Velocity onto an Inverted Flat Surface

Once the concentration boundary layer thickness is determined for the given values of  $L_i$ ,  $U$ ,  $\nu$ ,  $\mu$ ,  $d_p$ , and  $\rho_p$ , the mean flow velocity in  $z$ -direction within the concentration boundary layer, i.e.,  $\bar{u}_{c,i}$ , is obtained using Equation (6). For a flat surface, a unit width is assumed in  $x$ -direction, i.e.,  $\Delta x = 1$  and  $n_x = 1$  (Figure 6), where  $n_x$  is the number of grids in  $x$ -direction. The flow rate injected within the concentration boundary layer is

$$Q_{\text{in}} = \bar{u}_{c,i} \delta_{c,i}, \quad [19]$$

where the subscript “in” denotes particle injection. As a numerical procedure, the concentration boundary layer is divided into  $n_y$  elements with a constant spacing of

$$\Delta y_i = \frac{\delta_{c,i}}{n_y}. \quad [20]$$

Then, the initial location of each particle at the leading edge, i.e., the value of  $y$  for the center of each element (Figure 6a) is expressed as

$$y_{ij} = (j - 0.5)\Delta y_i \quad (j = 1, 2, 3, \dots, n_y). \quad [21]$$

The fraction making a contribution to particle deposition on the flat surface, out of the flow rate injected through the

infinitesimal area of  $\Delta y_i$  located at  $y_{ij}$ , is estimated as  $(Q_{de})_{ij} = \bar{u}_{c,i} \Delta y_i f_{ij}$ , where the subscript “de” denotes particle deposition and  $f_{ij}$  is calculated by repeating the procedure explained in Section 2.2 for every  $y_{ij}$ . Then, the total flow rate influencing particle deposition is

$$Q_{de} = \bar{u}_{c,i} \Delta y_i \sum_{j=1}^{n_y} f_{ij} \quad [22]$$

By assuming a homogeneous aerosol concentration, the number of particles ( $N$ ) is in proportion to the flow rate ( $Q$ ), i.e.,  $N_{de}/N_{in} = Q_{de}/Q_{in}$ . The deposition velocity ( $v_d$ ) onto an inverted flat surface in a parallel flow is obtained as

$$v_{d,FS} = \frac{J}{C_\infty} = \frac{N_{de}}{N_{in}} \cdot \frac{Q_{in}}{A_{de}} = \frac{Q_{de}}{A_{de}} = \frac{\bar{u}_{c,i} \Delta y_i}{L_i} \sum_{j=1}^{n_y} f_{ij}, \quad [23]$$

where the subscript “FS” denotes flat surface,  $J$  is the particle flux toward the deposition surface,  $C_\infty$  is the free-stream aerosol concentration, and  $A_{de}(= 1 \times L_i = L_i)$  is the area of deposition surface.

#### 2.4. Calculation of Deposition Velocity onto an Inverted Flat Surface of Finite Dimensions

In this section, a flat surface having finite dimensions, e.g., a wafer or a photomask, is considered. Figure 6b shows the top-view of a circular flat plate representing a wafer. Figures 6c and d display the top-views of square flat plates simulating the EUVL photomasks, one with its side facing the flow and the other with its corner confronting the flow, respectively. All these flat plates are inverted and exposed to a parallel flow. Due to the symmetric geometries, the half of the deposition area is taken into account for each plate shape and divided into  $n_x$  strip elements as shown in Figures 6b–d with a constant width of  $\Delta x$ . Then, each strip element is treated as a flat surface having the length of  $L_i$  as described in Section 2.3. For each plate shape, the length  $L_i$  and width  $\Delta x$  of the strip elements are expressed as follows.

For the circular flat plate (Figure 6b),

$$L_i = 2\sqrt{\left(\frac{D_w}{2}\right)^2 - x_i^2}, \quad [24]$$

$$\Delta x = \frac{D_w/2}{n_x} = \frac{D_w}{2n_x}, \quad [25]$$

where  $D_w$  is the wafer diameter. For the square flat plate with its side facing the flow (Figure 6c),

$$L_i = W, \quad [26]$$

$$\Delta x = \frac{W/2}{n_x} = \frac{W}{2n_x}, \quad [27]$$

where  $W$  is the photomask size. For the square flat plate with its corner confronting the flow (Figure 6d),

$$L_i = 2\left(\frac{W}{\sqrt{2}} - x_i\right), \quad [28]$$

$$\Delta x = \frac{(\sqrt{2}W)/2}{n_x} = \frac{W}{\sqrt{2}n_x}. \quad [29]$$

Here,  $x_i$  is the distance between each strip element and the centerline, and expressed as

$$x_i = (i - 0.5)\Delta x \quad (i = 1, 2, \dots, n_x). \quad [30]$$

Similar to the approach taken in Section 2.3 with the assumption of a homogeneous aerosol concentration, the ratio of the number of particles deposited on the surface to that injected within the concentration boundary layer is replaced by the ratio of the flow rate contributing to particle deposition to that entering within the concentration boundary layer, i.e.,  $N_{de,FFS}/N_{in,FFS} = Q_{de,FFS}/Q_{in,FFS}$ , where the subscript “FFS” denotes finite flat surface. Out of the flow rate going through the infinitesimal area of  $\Delta x \Delta y_i$  (Figure 6a), the flow rate contributing to particle deposition is  $(Q_{de,FFS})_{ij} = \bar{u}_{c,i} \Delta x \Delta y_i f_{ij}$ . Here,  $\bar{u}_{c,i}$  is the mean flow velocity within  $\delta_{c,i}$  corresponding to each strip element of the length  $L_i$ , and  $\delta_{c,i}$  is determined by the procedure described in Section 2.2. Then, the total flow rate affecting particle deposition on all strip elements is

$$Q_{de,FFS} = \sum_{i=1}^{n_x} \sum_{j=1}^{n_y} (Q_{de,FFS})_{ij} = \sum_{i=1}^{n_x} \sum_{j=1}^{n_y} \bar{u}_{c,i} \Delta x \Delta y_i f_{ij}. \quad [31]$$

The total flow rate entering within  $\delta_{c,i}$  for all strip elements is

$$Q_{in,FFS} = \sum_{i=1}^{n_x} \bar{u}_{c,i} \delta_{c,i} \Delta x. \quad [32]$$

Considering the symmetric geometries, the half areas of the wafer and the photomask are

$$A_{de,wafer} = \frac{\pi D_w^2}{8}, \quad [33]$$

$$A_{de,photomask} = \frac{W^2}{2}. \quad [34]$$

Similar to Equation (23), the deposition velocity onto a finite flat surface is calculated as  $v_{d,FFS} = Q_{de,FFS}/A_{de}$ . Using the appropriate expression of  $A_{de}$ , the deposition velocities onto the inverted wafer and photomask in a parallel flow are determined

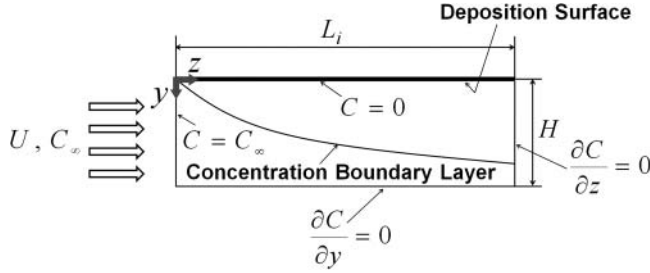


FIG. 7. Boundary conditions for solving convective diffusion equation [Equation (37)].

as

$$v_{d,waf er} = \frac{Q_{de,FFS}}{A_{de,waf er}} = \frac{8}{\pi D_w^2} \sum_{i=1}^{n_x} \sum_{j=1}^{n_y} \bar{u}_{c,i} \Delta x \Delta y_i f_{ij}, \quad [35]$$

$$v_{d,photomask} = \frac{Q_{de,FFS}}{A_{de,photomask}} = \frac{2}{W^2} \sum_{i=1}^{n_x} \sum_{j=1}^{n_y} \bar{u}_{c,i} \Delta x \Delta y_i f_{ij}. \quad [36]$$

### 3. NUMERICAL SIMULATION

Flow and aerosol-concentration fields are numerically simulated to validate the GDSM for the face-down flat surface, by assuming a steady state and two-dimensional aerosol flow in  $y$ - and  $z$ -directions. The velocity profile underneath the face-down flat surface is obtained using Equation (4). The aerosol-concentration distribution is determined by solving the equation of convective diffusion (Friedlander 2000). Since the gravity works against particle deposition as shown in Figure 3b and the flow velocity in  $y$ -direction is assumed to be zero, i.e.,  $w = 0$ , the equation of convective diffusion reduces to

$$D \left( \frac{\partial^2 C}{\partial y^2} + \frac{\partial^2 C}{\partial z^2} \right) - v_s \frac{\partial C}{\partial y} - u \frac{\partial C}{\partial z} = 0, \quad [37]$$

where  $C$  is the aerosol concentration. Figure 7 shows the boundary conditions for solving Equation (37). When  $U = 5$  cm/s and  $L_i = 45$  cm, the diffusion boundary layer thickness for the  $0.003$ - $\mu\text{m}$ -particles, from Equation (14), is about  $2$  cm at  $T = 293.15$  K and  $P = 101.325$  kPa. Therefore, the height of the calculation domain is set high enough to include the concentration boundary layer at the trailing edge, i.e.,  $H = 2.5$  cm for  $d_p$  ranging from  $0.003$   $\mu\text{m}$  to  $0.1$   $\mu\text{m}$  or  $H = 1.0$  cm for  $d_p$  larger than  $0.1$   $\mu\text{m}$ . The number of grids in  $y$ -direction used for solving the convective diffusion equation is  $500$  for  $d_p$  ranging from  $0.003$   $\mu\text{m}$  to  $0.1$   $\mu\text{m}$  or  $40,000$  for  $d_p$  larger than  $0.1$   $\mu\text{m}$ , which results in a constant grid spacing ( $h$ ) of  $50$   $\mu\text{m}$  or  $0.25$   $\mu\text{m}$  in  $y$ -direction, respectively. Once the aerosol concentration field is solved, the deposition velocity is calculated from the

average concentration gradient right underneath the deposition surface at  $y = h$  as

$$v_{d,FS,sim} = \frac{J}{C_\infty} = \frac{D}{C_\infty} \cdot \left( \frac{\partial C}{\partial y} \right)_{y=h}, \quad [38]$$

where the subscript “sim” denotes simulation and the local concentration gradient  $(\partial C / \partial y)_{y=h}$  is averaged over the plate area of  $L_i$ . The local concentration gradient is determined by the forward finite-divided-difference formula (Chapra and Canale 1998), which uses the values of aerosol concentration at three nodal points, i.e.,

$$\left( \frac{\partial C}{\partial y} \right)_{y=h} = \frac{-3C_1 + 4C_2 - C_3}{2h}, \quad [39]$$

where  $C_1$ ,  $C_2$ , and  $C_3$  are the values of aerosol concentration underneath the deposition surface at  $y = h$ ,  $y = 2h$ , and  $y = 3h$ , respectively.

## 4. RESULTS AND DISCUSSION

### 4.1. Validation of GDSM for Inverted Flat Surfaces

C and FORTRAN codes were developed to compute the deposition velocity onto the inverted flat surface by the GDSM and the simulation, as explained in Sections 2 and 3, respectively. Figure 8 shows the comparison of deposition velocity onto an inverted flat surface with the length of  $L_i = 45$  cm, between the predictions by the GDSM [Equation (23)] and the simulation [Equation (38)], when Brownian diffusion and gravitational settling were simultaneously considered. Spherical particles of unit density, i.e.,  $\rho_p = 1$  g/cm<sup>3</sup>, were assumed. The ambient pressure and temperature were  $101.325$  kPa and  $293.15$

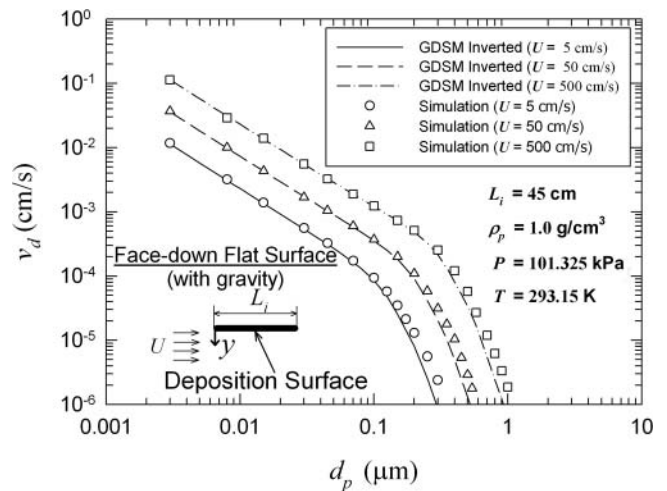


FIG. 8. Comparison of deposition velocities for a 45-cm-long flat plate between the GDSM [Equation (23)] and the flow-aerosol-concentration simulation [Equation (38)].



K, respectively. The free-stream air velocities were 5, 50, and 500 cm/s by taking into account the speeds of wafer/photomask transportation in the cleanroom. The Reynolds number ranged from approximately 1,500 to 150,000, i.e., the flow was laminar. In the GDSM, the deposition velocities were found to converge with the percent relative error of 0.03%, when  $n_\sigma = 6$ ,  $n_y = 256$ ,  $n_t = 100$  and  $\varepsilon_s = 10^{-4}$ . The GDSM data agreed very well with the simulation results for particle sizes ranging from 0.003  $\mu\text{m}$  to 0.1  $\mu\text{m}$ . When  $d_p$  was larger than approximately 0.1  $\mu\text{m}$ , the discrepancy in deposition velocity between the GDSM and the simulation became larger as the particle size increased. One of the reasons for the discrepancy might be the overestimation of deposition velocity calculated by the simulation, due to the artificial diffusion that generally occurs when solving the equation of convective diffusion with the Eulerian approach (Laval et al. 2003). In other words, non-zero values of aerosol concentration would be assigned to the grids underneath the deposition surface near the trailing edge, even though no particles of large size might reach the surface near the trailing edge, as can be conjectured from Figure 3b. In spite of the discrepancy, the tendencies of deposition velocity were similar. The deposition velocity onto the inverted flat surface decreased with increasing  $d_p$ . For the particle size larger than approximately 0.1  $\mu\text{m}$ , the deposition velocity dropped markedly with a steep gradient, which implies that the inverted orientation of the wafer or photomask is helpful for reducing particulate contamination during transportation, especially for large particle sizes.

To validate the GDSM for the inverted finite flat surface, Figure 9 compares the mean mass transfer coefficients ( $h_{\text{mass}}$ ) for the circular or square flat surfaces, i.e., the deposition velocities only due to Brownian diffusion, between the prediction by the GDSM [Equation (35) or (36)] and that by the mass transfer correlation of Yook et al. (2010a), which is valid in laminar flow regime and expressed as

$$h_{\text{mass}} = B \text{Re}_{L_c}^{1/2} \text{Sc}^{1/3} \frac{D}{L_c}, \quad [40]$$

where  $B$  is the correlation constant,  $\text{Re}_{L_c} (= UL_c/\nu)$  is the Reynolds number, and  $L_c$  is the streamwise characteristic length. The value of  $B$  and the definition of  $L_c$  are listed in Table 1 according to plate shape. Note that the gravity was omitted in the GDSM, i.e.,  $v_s = 0$ , to calculate the mean mass transfer coefficient. The free-stream air velocity varied from 5 to 500 cm/s. The ambient pressure and temperature were 101.325 kPa and 293.15 K, respectively. The particles were assumed to be spherical and of unit density. It was found that the GDSM for the inverted finite flat surface produced converged data with the percent relative error of 0.02%, when  $n_\sigma = 6$ ,  $n_x = 256$ ,  $n_y = 256$ ,  $n_t = 100$ , and  $\varepsilon_s = 10^{-4}$ . Figure 9a shows the comparison of mean mass transfer coefficients between the GDSM [Equation (35)] and the correlation of Yook et al. (2010a) [Equation (40)] for a circular flat surface with the diameter of  $D_w = 45$  cm. Figures 9b and c compares mean mass transfer coefficients

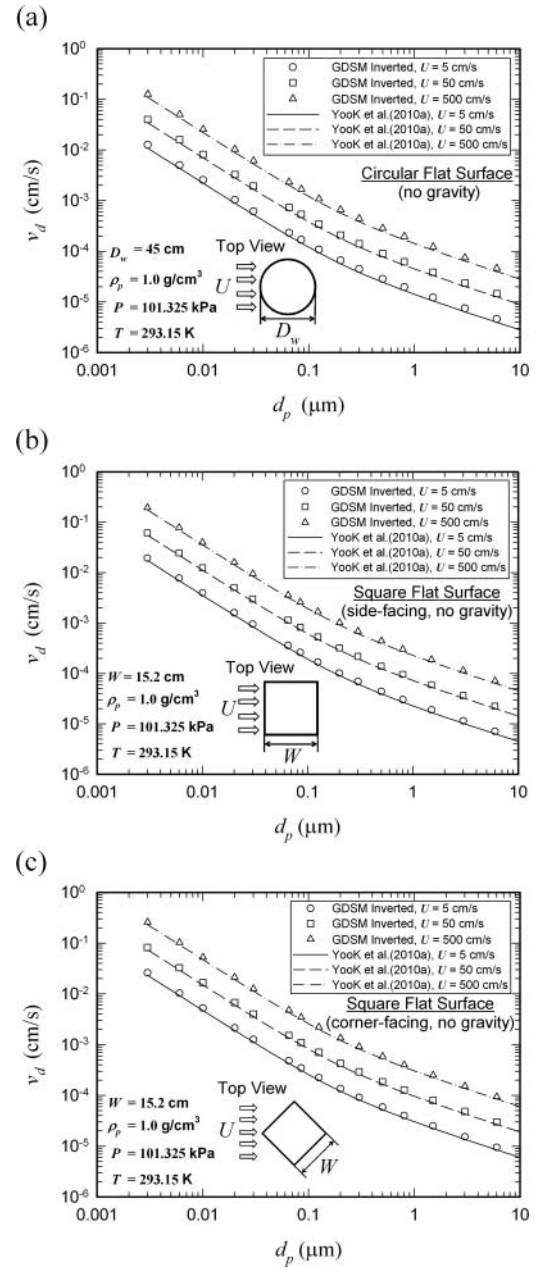
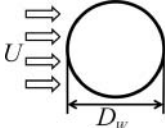
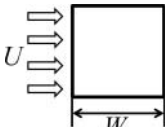
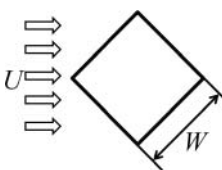


FIG. 9. Comparison of deposition velocities for a finite flat surface between the GDSM [Equation (35) or Equation (36)] considering only Brownian diffusion, i.e.,  $v_s = 0$ , and the mass transfer correlation of Yook et al. (2010a) [Equation (40)]: (a) a circular flat surface with the diameter of  $D_w = 45$  cm; (b) a side-facing square flat surface with the size of  $W = 15.2$  cm; (c) a corner-facing square flat surface with the size of  $W = 15.2$  cm.

between the GDSM [Equation (36)] and the correlation of Yook et al. (2010a) [Equation (40)] for a side-facing square flat surface and a corner-facing square flat surface, respectively, with the length of  $W = 15.2$  cm. The agreement between the GDSM (with  $v_s = 0$ ) for the inverted finite flat surface and the correlation of Yook et al. (2010a) was good over the tested particle size ranging from 0.003  $\mu\text{m}$  to 10  $\mu\text{m}$ .

TABLE 1  
Correlation constant and streamwise characteristic length definition for the mass transfer correlation of Yook et al. (2010a) [Equation (40)]

Plate shape (Top-view)	Correlation constant ( $B$ )	Streamwise characteristic length ( $L_c$ )
	0.769	$D_w$
	0.691	$W$
	0.921	$\sqrt{2} W$

In summary, Figure 8 shows that the GDSM for the inverted flat surface can correctly predict the deposition velocity under the effects of Brownian diffusion and gravitational settling, and Figure 9 implies that the procedure of integrating deposition probabilities by dividing the finite flat surface into many strip elements and considering each strip element as a flat surface is reasonable for finding out the deposition velocities for the inverted flat surfaces of various areal shapes with finite dimensions.

#### 4.2. Deposition Velocity onto an Inverted Wafer or Photomask

Based on the validation results, the deposition velocity onto an inverted wafer or photomask was predicted by considering both Brownian diffusion and gravitational settling of aerosol particles. Transportation speeds of the wafer or photomask varied from 5 to 500 cm/s at the ambient conditions of 101.325 kPa and 293.15 K. Spherical particles of unit density were assumed. The constants used for the GDSM calculation were  $n_\sigma = 6$ ,  $n_x = 256$ ,  $n_y = 256$ ,  $n_t = 100$  and  $\varepsilon_s = 10^{-4}$ .

Figure 10 shows the deposition velocity onto an inverted wafer surface in a parallel flow, predicted by the GDSM [Equation (35)], when the wafer diameter was  $D_w = 45$  cm, which is going to be adopted in semiconductor manufacturing in the year 2012 according to the International Technology Roadmap for Semiconductors 2007. The tendency of deposition velocity onto the inverted wafer was similar to that onto the inverted flat surface illustrated in Figure 8. Namely, the deposition velocity decreased with increasing particles size, especially with a steep gradient for the particles larger than about 0.1  $\mu\text{m}$ .

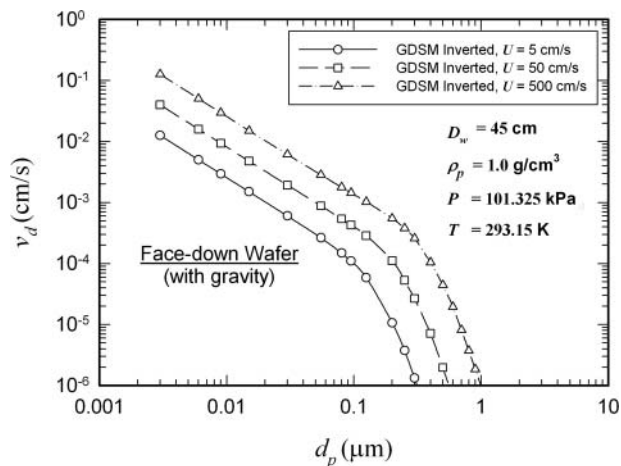


FIG. 10. Deposition velocities onto the 45-cm-wafer, predicted by the GDSM [Equation (35)].

Figure 10 illustrates that the inverted orientation of the wafer is helpful for reducing particulate contamination during horizontal transportation and that the particles larger than about 1  $\mu\text{m}$  can hardly deposit on the face-down critical surface.

Figure 11 compares the deposition velocities onto the inverted square flat surfaces, simulating the EUVL photomasks, between the side-facing (Figure 6c) and corner-facing (Figure 6d) orientations in a parallel flow. According to the SEMI Standard P37-1102, the EUVL photomask size is  $W = 15.2$  cm and its thickness is 0.635 cm. For the qualitative comparison of deposition velocity between the two orientations, the effect of photomask thickness was unconsidered. When the inverted square flat surface confronted the flow with its corner, the deposition velocities in diffusion-dominant regime were higher by 12% compared with the case when it faced the flow with its

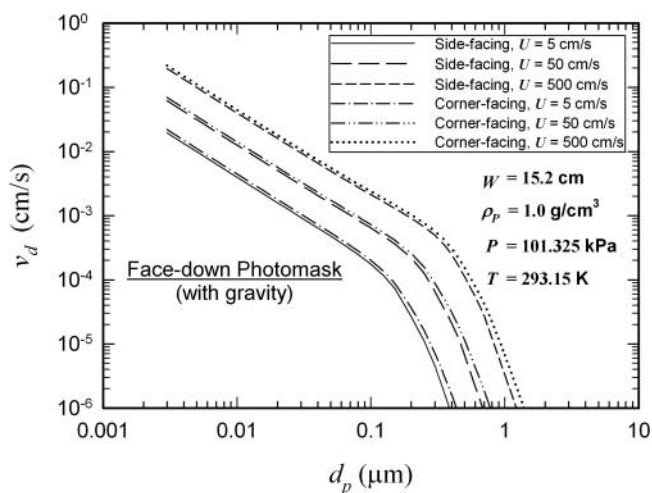


FIG. 11. Qualitative comparison of deposition velocities onto the 15.2-cm-EUVL-photomask between the side-facing and the corner-facing orientations, predicted by the GDSM [Equation (36)].

side, and the difference in deposition velocity between two photomask orientations became larger with increasing particle size, in the tested free-stream velocity range. To qualitatively explain this phenomenon, the mean characteristic length, i.e., the average of streamwise-length per unit spanwise-width of all strip elements (Figure 6), was calculated as follows: For the side-facing photomask orientation, from Equation (26) and Equation (27),

$$\begin{aligned} \left(\frac{L_i}{\Delta x}\right)_{\text{avg}} &= \frac{1}{n_x} \int_0^{W/2} \left(\frac{L_i}{\Delta x}\right) dx \\ &= \frac{1}{n_x} \int_0^{W/2} \left[\frac{W}{W/(2n_x)}\right] dx = W. \end{aligned} \quad [41]$$

For the corner-facing photomask orientation, from Equations (28) and (29),

$$\begin{aligned} \left(\frac{L_i}{\Delta x}\right)_{\text{avg}} &= \frac{1}{n_x} \int_0^{W/\sqrt{2}} \left(\frac{L_i}{\Delta x}\right) dx \\ &= \frac{1}{n_x} \int_0^{W/\sqrt{2}} \left[\frac{2(W/\sqrt{2}-x)}{W/(\sqrt{2}n_x)}\right] dx = \frac{\sqrt{2}}{2} W. \end{aligned} \quad [42]$$

By comparing the results in Equation (41) and Equation (42), the mean characteristic length for the corner-facing orientation was shorter than that for the side-facing orientation. Since the deposition velocity is highest at the leading edge and decreases with increasing plate length as the convective heat and mass transfer coefficients do, the corner-facing orientation is expected to show higher deposition velocity than the side-facing orientation. This suggests that the side-facing scheme in addition to the inverted orientation is helpful for minimizing the particulate contamination of EUVL photomasks during horizontal transportation.

## 5. CONCLUSIONS

The Gaussian Diffusion Sphere Model was improved and adjusted for predicting the deposition velocity onto an inverted flat surface in a parallel flow. The GDSM for an inverted flat surface was validated by comparing with the simulation of solving the flow and aerosol-concentration fields under the consideration of Brownian diffusion and gravitational settling of aerosol particles. The GDSM procedure of integrating the deposition probabilities for an inverted finite flat surface, of which areal shape was circular or square, was verified by comparing the deposition velocities computed by the GDSM assuming no gravity with the mean mass transfer coefficients obtained from the correlation of Yoon et al. (2010a). The validation results showed that the GDSM could correctly predict the deposition velocity onto the inverted finite flat surfaces. In addition to the accuracy, the GDSM had another advantage of fast prediction compared

with the simulation of solving flow and aerosol-concentration fields. For example, it took one hour for the GDSM to obtain the deposition velocities onto an inverted 45-cm-wafer surface for 20 particle sizes, i.e., each single curve shown in Figure 10, when a 2.66-GHz-CPU personal computer was used.

The GDSM was used to predict the deposition velocities onto the inverted circular flat surface, representing the 45-cm-wafer, or the inverted square flat surfaces, simulating the 15.2-cm-EUVL photomasks one with side-facing and the other with corner-facing orientation. It was shown that the scheme of transporting the wafer or EUVL photomask with the critical surface facing-down was helpful for minimizing the particulate contamination, especially for large particle sizes. In addition, from the qualitative comparison of deposition velocities between the two representative photomask orientations in a parallel flow, it was found that the scheme of side-facing transportation could render the critical surface of the EUVL photomask less contaminated.

In this study, only the gravitational settling velocity was taken into account as the drift velocity of particles moving away from the surface in  $y$ -direction. It is expected that the cases of repelling particles away from a flat surface in a parallel flow by electrophoresis, maybe even thermophoresis, can be treated using the adjusted GDSM presented in this study, by considering electrophoretic or thermophoretic migration velocity in Equation (9).

## NOMENCLATURE

$A$	deposition surface area
$B$	correlation constant
$C$	aerosol concentration
$C_c$	slip correction factor
$D$	particle diffusivity
$D_w$	wafer diameter
$d_p$	particle diameter
$f$	deposition probability
$G$	distance between GDS center and deposition surface
$g$	gravitational acceleration
$H$	height of calculation domain
$h$	constant grid spacing
$h_{\text{mass}}$	mean mass transfer coefficient
$J$	particle flux
$L$	plate length
$L_c$	streamwise characteristic length
$N$	number of particles
$n_t$	number of grids in time domain
$n_x$	number of elements in $x$ -direction
$n_y$	number of elements in $y$ -direction
$n_\sigma$	integer for determining confidence interval
$P$	ambient pressure
$Q$	flow rate
$R$	radius of GDS
Re	Reynolds number
Sc	Schmidt number

$T$	ambient temperature
$t$	residence time
$U$	free-stream velocity in $z$ -direction
$u$	velocity in $z$ -direction
$\bar{u}_c$	mean velocity in $z$ -direction within concentration boundary layer
$v_d$	deposition velocity
$v_s$	settling velocity
$W$	photomask size
$w$	velocity in $y$ -direction
$x, y, z$	coordinates
$Y$	upper limiting trajectory of GDS

### Greek Symbols

$\Delta$	increment
$\delta_c$	concentration boundary layer thickness
$\delta_d$	diffusion boundary layer thickness
$\delta_f$	flow boundary layer thickness
$\delta_s$	settling distance
$\varepsilon_a$	percent relative error
$\varepsilon_s$	prespecified acceptable level
$\mu$	viscosity of air
$\nu$	kinematic viscosity of air
$\rho_p$	particle density
$\sigma$	standard deviation

### Subscripts

de	deposition
$i$	$i$ -th element in $x$ -direction
in	injection
inf	point of inflection
$j$	$j$ -th element in $y$ -direction
$k$	previous value in iterative calculation
$k+1$	current value in iterative calculation
$\infty$	free-stream

### REFERENCES

- Asbach, C., Fissan, H., Kim, J. H., Yook, S. J., and Pui, D. Y. H. (2006). Technical Note: Concepts for Protection of EUVL Masks from Particle Contamination. *J. Nanopart. Res.* 8:705–708.
- Asbach, C., Stahlmecke, B., Fissan, H., Kuhlbusch, T. A. J., Wang, J., and Pui, D. Y. H. (2008). Analytical-statistical model to accurately estimate diffusional nanoparticle deposition on inverted surfaces at low pressure. *Appl. Phys. Lett.* 92:064107.
- Cengel, Y. A. (2003). *Heat Transfer: A Practical Approach*. 2nd ed., McGraw-Hill, New York, p. 354, 755.
- Chapra, S. C., and Canale, R. P. (1998). *Numerical Methods for Engineers*. 3rd ed., McGraw-Hill, New York, p. 630.
- Friedlander, S. K. (2000). *Smoke, Dust, and Haze: Fundamentals of Aerosol Dynamics*. 2nd ed., Oxford University Press, New York, p. 59.
- Hinds, W. C. (1999). *Aerosol Technology: Properties, Behavior, and Measurement of Airborne Particles*. 2nd ed., John Wiley, New York, p. 49, 158.
- Holman, J. P. (2010). *Heat Transfer*. 10th ed., McGraw-Hill, New York, p. 226.
- Kemp, K., and Wurm, S. (2006). EUV Lithography. *C. R. Physique* 7:875–886.
- Lai, A. C. K., and Nazaroff, W. W. (2000). Modeling Indoor Particle Deposition from Turbulent Flow onto Smooth Surfaces. *J. Aerosol Sci.* 31: 463–476.
- Liu, B. Y. H., and Ahn, K. H. (1987). Particle Deposition on Semiconductor Wafers. *Aerosol Sci. Technol.* 6:215–224.
- Opiolka, S., Schmidt, F., and Fissan, H. (1994). Combined Effects of Electrophoresis and Thermophoresis on Particle Deposition onto Flat Surfaces. *J. Aerosol Sci.* 25:665–671.
- Otani, Y., Emi, H., Kanaoka, C., and Kato, K. (1989). Determination of Deposition Velocity onto a Wafer for Particles in the Size Range between 0.03 and 0.8  $\mu\text{m}$ . *J. Aerosol Sci.* 20:787–796.
- Pui, D. Y. H., Ye, Y., and Liu, B. Y. H. (1990). Experimental Study of Particle Deposition on Semiconductor Wafers. *Aerosol Sci. Technol.* 12: 795–804.
- Wood, N. B. (1981). A Simple Method for the Calculation of Turbulent Deposition to Smooth and Rough Surfaces. *J. Aerosol Sci.* 12:275–290.
- Ye, Y., Pui, D. Y. H., Liu, B. Y. H., Opiolka, S., Blumhorst, S., and Fissan, H. (1991). Thermophoretic Effect of Particle Deposition on a Free Standing Semiconductor Wafer in a Clean Room. *J. Aerosol Sci.* 22:63–72.
- Yook, S. J., Fissan, H., Asbach, C., Kim, J. H., Dutcher, D. D., Yan, P. Y., and Pui, D. Y. H. (2007a). Experimental Investigations on Particle Contamination of Masks without Protective Pellicles during Vibration or Shipping of Mask Carriers. *IEEE Trans. Semicond. Manuf.* 20:578–584.
- Yook, S. J., Fissan, H., Asbach, C., Kim, J. H., Wang, J., Yan, P. Y., and Pui, D. Y. H. (2007b). Evaluation of Protection Schemes for Extreme Ultraviolet Lithography (EUVL) Masks against Top-Down Aerosol Flow. *J. Aerosol Sci.* 38:211–227.
- Yook, S. J., Fissan, H., Asbach, C., Kim, J. H., van der Zwaag, T., Engelke, T., Yan, P. Y., and Pui, D. Y. H. (2007c). Experimental Investigations of Protection Schemes for Extreme Ultraviolet Lithography Masks in Carrier Systems against Horizontal Aerosol Flow. *IEEE Trans. Semicond. Manuf.* 20:176–186.
- Yook, S. J., and Ahn, K. H. (2009). Gaussian Diffusion Sphere Model to Predict Mass Transfer due to Diffusional Particle Deposition on a Flat Surface in Laminar Flow Regime. *Appl. Phys. Lett.* 94:191909.
- Yook, S. J., Hwang, H. J., Lee, K. S., and Ahn, K. H. (2010a). Particle Deposition Velocity onto a Wafer or a Photomask in a Laminar Parallel Flow. *J. Electrochem. Soc.* 157:H692–H698.
- Yook, S. J., Asbach, C., and Ahn, K. H. (2010b). Particle Deposition Velocity onto a Face-up Flat Surface in a Laminar Parallel Flow Considering Brownian Diffusion and Gravitational Settling. *J. Aerosol Sci.* doi:10.1016/j.jaerosci.2010.06.003 (in press).
- Zhao, B., and Wu, J. (2006a). Modeling Particle Deposition from Fully Developed Turbulent Flow in Ventilation Duct. *Atmos. Environ.* 40: 457–466.
- Zhao, B., and Wu, J. (2006b). Modeling Particle Deposition onto Rough Walls in Ventilation Duct. *Atmos. Environ.* 40:6918–6927.